


Article

Nanostructured Ceramic Photocatalytic Membrane Modified with a Polymer Template for Textile Wastewater Treatment

Rizwan Ahmad ^{1,†}, Jin Kyu Kim ^{2,†}, Jong Hak Kim ^{2,*}  and Jeonghwan Kim ^{1,*}

¹ Department of Environmental Engineering, Inha University, Inharo-100, Namgu, Incheon 402751, Korea; rizwanahmad.ra89@gmail.com

² Department of Chemical and Biomolecular Engineering, Yonsei University, 50 Yonsei-ro, Seodaemun-gu, Seoul 03722, Korea; jkk4885@gmail.com

* Correspondence: jonghak@yonsei.ac.kr (J.H.K.); jeonghwankim@inha.ac.kr (J.K.); Tel: +82-32-860-7502 (J.K.)

† These authors contributed equally to this work.

Received: 5 November 2017; Accepted: 5 December 2017; Published: 9 December 2017

Abstract: Photocatalytic ceramic membranes have attracted considerable attention for industrial wastewater treatment. However, morphological control of the membrane surface to improve its photocatalytic reactivity for the degradation of organic pollutants remains a challenge. Herein, we report a new nanostructured TiO₂/Al₂O₃ composite ceramic membrane prepared from a poly(oxyethylene methacrylate) (POEM) template through a sol–gel method and its photocatalytic performance in the treatment of a model dye compound. The POEM polymeric template allowed the homogeneous distribution of catalytic sites, i.e., the TiO₂ layer, on the Al₂O₃ membrane surface, resulting in improved organic dye degradation along with effective fouling mitigation. The immobilization of a TiO₂ layer on the Al₂O₃ membrane support also significantly enhanced the membrane adsorption capacity toward dye organic compounds. An organic removal efficiency of over 96% was achieved with the TiO₂/Al₂O₃ composite membrane under Ultraviolet (UV) irradiation. In addition, the self-cleaning efficiency of the TiO₂/Al₂O₃ composite membrane was remarkably improved by the degradation of organic foulants on the membrane under UV illumination.

Keywords: photocatalytic membrane; antifouling; polymer template; TiO₂; adsorption

1. Introduction

The demand for advanced water treatment technologies is increasing for the treatment of high-strength wastewater, such as industrial wastewater including complex water pollutants. Membrane technology is a promising way to enhance wastewater treatment efficiency as it can produce great effluent (permeate) quality with a smaller footprint than that afforded by conventional wastewater treatment processes [1–3]. However, the polymeric membranes widely adopted in wastewater treatment applications display relatively low thermal and chemical resistance. There has been an upsurge of interest in ceramic membranes for the treatment of high-strength wastewater, for which polymeric membranes are not suitable [4,5]. Ceramic membranes consisting of metal oxides usually exhibit high membrane porosity, membrane permeability, and narrow distribution of the membrane pore size. These unique properties allow for superior separation characteristics and antifouling behavior than those of polymeric membranes.

Photocatalytic membrane reactors (PMRs) combine photocatalytic reactors with membrane filtration units [6,7]. As the photocatalytic membrane is combined with oxidation promoters, such as UV irradiation, the membrane plays an important role as a support for the photocatalytic materials and as a selective barrier to degrade organic contaminants. The TiO₂ materials are often considered

as coating materials on ceramic support for the photocatalytic membrane because of their high photocatalytic activity and thermal/chemical stability at low environmental toxicity [8–10]. The TiO_2 coating on the ceramic support has been reported to provide high water permeability with relatively low fouling rate to polymeric membrane [11,12]. The photo-degradation activity of nanostructured ceramic membranes functionalized in situ have been found to be very effective for wastewater treatment [9]. Thus, the photocatalytic layer on the membrane is expected to reduce the extent of membrane fouling while producing an excellent permeate quality due to the selective photocatalytic degradation of organic compounds on the catalytic membrane surface [13]. In addition, the intrinsic properties of the ceramic membrane against certain chemical reagents allow for the photocatalytic membrane to withstand the concomitant attack of the strong oxidants produced during photocatalytic processes, e.g., hydroxyl radicals [14].

The hierarchically porous nanostructure of the catalyst film on the ceramic membrane plays a critical role in determining the photocatalytic membrane performance. The morphology of the photocatalyst film on the membrane support has been found to be an important factor determining the membrane surface reactivity [15]. The introduction of surface-directing agents on the ceramic support has allowed the control of its porous structure [6,8,15,16]. For example, the porous structure of a photocatalyst film was enhanced using a Pluronic block copolymer for high organic dye removal efficiency [16]. Choi et al. [17] found that the mesoporous and narrow pore size distribution of photocatalyst films improve the wastewater treatment efficiency significantly. A grafted copolymer-based composite membrane exhibited excellent properties in terms of organic-compound degradation efficiency [15]. Homopolymers can also be used with great potential to improve the photocatalytic membrane reactivity. The photocatalytic activity of TiO_2 composite membranes has been significantly enhanced by introducing hydrophobic homopolymers consisting of polyvinyl chloride (PVC) as a polymer template in the membrane support [6]. Nevertheless, developing photocatalytic membranes with uniform distribution of catalytic materials on ceramic support with fine-tuned nanostructure is still major challenge.

Herein, we report the development of a nanostructured $\text{TiO}_2/\text{Al}_2\text{O}_3$ composite ceramic membrane using a poly(oxyethylene methacrylate) (POEM) template through a sol–gel method to improve the photocatalytic membrane reactivity for textile wastewater treatment application. The prepared membrane was characterized by scanning electron microscopy (SEM), atomic force microscopy (AFM), X-ray diffraction (XRD), and transmission electron microscopy (TEM). The adsorption behavior and antifouling performance were also systematically evaluated by filtering a model dye solution.

2. Materials and Methods

2.1. Materials

Poly(oxyethylene methacrylate) (POEM, poly(ethylene glycol) methyl ether methacrylate, number average molecular weight (M_n) = 500 g/mol), poly(vinyl pyrrolidone) (PVP, average molecular weight = 40,000 g/mol), titanium(IV) isopropoxide (TTIP, 97%), and a hydrogen chloride solution (37 wt %) were purchased from Sigma-Aldrich, Youngin, Korea. Absolute ethanol and tetrahydrofuran (THF) were bought from J. T. Baker. The alumina support ($\alpha\text{-Al}_2\text{O}_3$, thickness = 2 mm, diameter = 30 mm, pore size = 100 nm) was purchased from Nano Pore Materials Co., Ltd., Seoul, Korea. Milli-Q deionized water (resistivity: 18.2 M Ω and pH: 6.8) from ultrapure water production system (STS-8L, Human Science, Seoul, Korea) was used in experimental works performed in this study.

2.2. Membrane Fabrication

To prevent the penetration of the polymer/ TiO_2 precursor mixture solution into the membrane pores, a PVP ethanol solution (10 wt %) was spin-coated on the bare Al_2O_3 membrane at 500 rpm for 20 s and subsequently dried at 50 °C in an oven for the complete removal of ethanol. To prepare the TiO_2 precursor solution, HCl was slowly added to TTIP dropwise under vigorous stirring. Deionized

water was added to the solution and stirred for at least 30 min. POEM (0.03 g) was dissolved in 1.5 mL of THF (2 wt %) and mixed with 0.2 mL of the as-prepared TiO_2 precursor solution over 3 h for the sol-gel process. The mixed polymer/ TiO_2 precursor mixture solution was spin-coated on the PVP-coated Al_2O_3 membrane, followed by calcination at 450 °C for 30 min. After calcination, the organic materials such as POEM, PVP, and the solvents were removed and a crystalline TiO_2 film was obtained on the Al_2O_3 membrane.

2.3. Experimental Set-Up

The laboratory-scale, dead-end PMR is shown in Figure 1. The experimental set-up consisted of a membrane module integrated with a UV lamp, feed reservoir, and data acquisition system. A Congo red dye solution ($100 \text{ mg}\cdot\text{L}^{-1}$) was used to simulate the dye wastewater. The feed solution was prepared by diluting a stock solution of $500 \text{ mg}\cdot\text{L}^{-1}$. The test solution was placed in a 5 L feed reservoir under continuous stirring at a constant pressure of 1.5 bar applied by a pressurized oxygen tank to push the feed solution toward the membrane module equipped with a disk-type ceramic membrane (effective surface area of 4.5 cm^2). The aim of oxygen gas was to enhance the photocatalytic activity as it can act as an electron acceptor and thus can reduce the probability of electron hole recombination. A UV-C lamp ($\lambda_{\text{max}} = 254 \text{ nm}$, Philips TUV 4W SLM, Seoul, Korea) was installed inside the membrane module to irradiate UV light on membrane surface directly. The thickness of water channel between UV lamp and membrane surface was approximately 2 cm. The permeate water produced by the membrane module was collected in a permeate vessel and weighed on an electronic balance (Ohaus Corporation, Pine Brook, NJ, USA). The data acquisition system was used to monitor the permeate weight on the electronic balance with the filtration time. The permeate flux (LMH) ($\text{L m}^{-2} \text{ h}^{-1}$) was calculated by the permeate volume (L) divided by the effective membrane surface area (m^2) and filtration time (h). The concentration of Congo red in the membrane permeate was analyzed by measuring its absorbance (λ_{max}) at 496 nm using a UV-Visible spectrophotometer (SCINCO, S-3100, Seoul, Korea). Pure deionized water from an ultrapure water production system (STS-8I, Human Science, Seoul, Korea) was used in all the experimental work performed in this study.

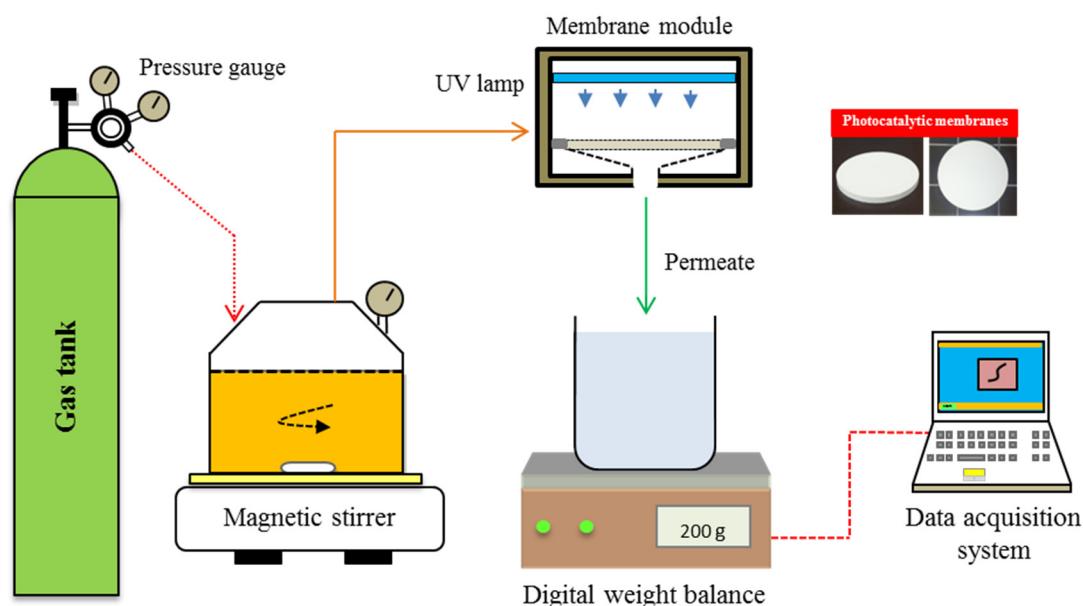


Figure 1. Experimental setup of the photocatalytic membrane reactor (PMR) with direct ultraviolet (UV) irradiation on membrane surface.

2.4. Photocatalytic Performance of the Membranes

The adsorption capacity of the bare Al_2O_3 and $\text{TiO}_2/\text{Al}_2\text{O}_3$ composite membranes was examined by filtering a feed solution under dark conditions (i.e., without UV illumination). To evaluate the antifouling properties and photocatalytic activity of the membranes, filtrations were performed under UV illumination in dead-end filtration mode. All experimental works were carried out at least three times to confirm result reproducibility. The membranes were cleaned chemically after each experiment by placing them in a 1 mole/L NaOH solution (98% Beads, SAMCHUN Pure Chemicals Co., Ltd. Seoul, Korea) for 5 min and then in deionized water for 12 h. In order to know effect of temperature on membrane permeability, the permeability measured experimentally was compared with the one calculated by Darcy's equation below at elevated temperature in permeate line under UV radiation at the end of filtration.

$$J = \frac{\Delta P}{\mu R_m} \quad (1)$$

where J represents membrane permeate flux ($\text{L m}^{-2} \text{h}^{-1}$), ΔP is the trans-membrane pressure (bar), R_m is the membrane resistance (m^{-1}), and μ represents viscosity ($\text{Pa}\cdot\text{s}$) of pure water at specific temperature.

2.5. Analytical Methods for Membrane Characterization

The surface and cross-section morphologies of the TiO_2 film on the Al_2O_3 membrane and the bare Al_2O_3 membrane were investigated by field emission SEM (FE-SEM, SUPRA 55VP, Carl Zeiss, Germany/FE-SEM, JSM-7001F, JEOL Ltd., Tokyo, Japan). The crystalline phase of the composite membranes was characterized by XRD (generator: 40 kV, 40 mA, D8 ADVANCE with DAVINCI, BRUKER, Bremen, Germany, wavelength (λ): $\text{Cu K}\alpha_1$ (\AA)-1.5418 \AA , two theta range: $10\text{--}80^\circ$). The morphology and crystallinity of the TiO_2 structure detached from the fluorine-doped tin oxide (FTO) glass by scratching the slide glass were analyzed by high resolution-TEM (HR-TEM, JEM-3010, JEOL, Tokyo, Japan). The 3D surface morphology of the TiO_2 film on the Al_2O_3 membrane was characterized by AFM (XE-Bio, Park Systems, Suwon, Korea).

3. Results and Discussion

3.1. Membrane Morphology

The nanostructure morphology of a membrane has a great effect on its photocatalytic performance for wastewater treatment. Polymer templates are considered effective structure-directing agents for the control of the nanostructure morphology. They not only effectively induce the organized structure of a membrane, but also have no negative impact on the membrane performance due to its complete degradation upon calcination. Since the hydrophilic TiO_2 precursor TTIP has high affinity toward hydrophilic materials, it interacts strongly with the hydrophilic POEM chains. A POEM/TTIP hybrid was thus successfully formed during the sol-gel process. Since the low-viscosity POEM/TTIP solution can easily penetrate the macroporous Al_2O_3 membrane, its presence will influence the nanostructure morphology and, subsequently, the membrane performance. Our previous study showed that polymeric template/TTIP solution could be penetrated into the pore structure of macroporous Al_2O_3 support and it caused non-uniform photocatalytic film on the ceramic support [15]. With the help of a PVP coating on the Al_2O_3 membrane [6,15], the penetration of the POEM/TTIP solution deep inside the membrane was prevented and a TiO_2 thin film was thereby successfully obtained. During calcination at 450°C , TTIP was transformed into crystalline TiO_2 , while the organic POEM, PVP, and solvents were all completely decomposed. The synthesized TiO_2 film on the Al_2O_3 membrane was found to be highly crystalline and well organized [15,18].

The surface of the TiO_2 structure on the FTO glass and Al_2O_3 membrane was characterized by SEM analysis (Figure 2). A uniform TiO_2 film prepared with the aid of POEM was successfully synthesized on a flat FTO glass substrate. Owing to the nonporous substrate and strong interactions

between TTIP and POEM, the TiO_2 film exhibits a well-organized morphology, as shown in Figure 2a. The bare membrane with a pore size of approximately 100 nm is clearly observed in Figure 2b. Large Al_2O_3 crystals are also observed in the magnified surface image in Figure 2c. The morphology of the POEM-directed TiO_2 structure on the Al_2O_3 membrane in Figure 2d is similar to that of the bare membrane. This is attributable to the formation of a very thin TiO_2 film resulting from the low-viscosity POEM/TTIP solution. In the enlarged image shown in Figure 2e, the Al_2O_3 crystals appear well covered with uniform and well-connected TiO_2 nanoparticles consisting of the POEM/TTIP hybrid.

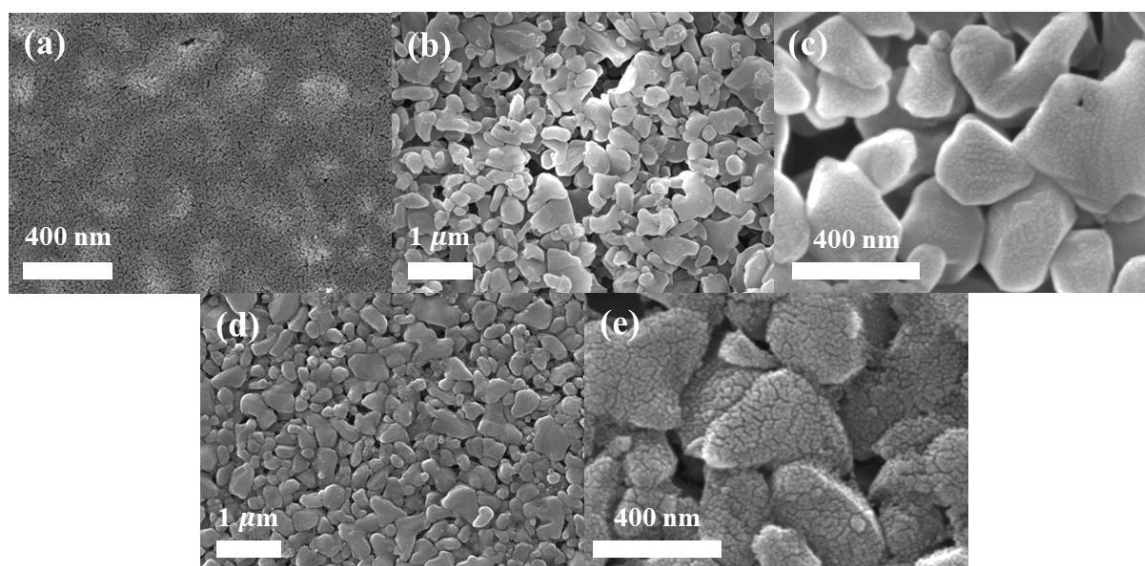


Figure 2. Surface scanning electron microscopy (SEM) image of a (a) Poly(oxyethylene methacrylate) (POEM)-directed TiO_2 film on FTO glass; (b,c) the bare Al_2O_3 membrane; and (d,e) the POEM-directed TiO_2 film on the Al_2O_3 membrane.

The distribution of TiO_2 on Al_2O_3 membrane was investigated with EDS analysis (Figure 3). The Ti elemental mapping image of TiO_2 structure prepared by the POEM template revealed that TiO_2 was homogeneously distributed on the entire surface of Al_2O_3 membrane. The aggregation of photocatalysts on membrane should be prevented for effective photocatalysis and high permeate flux. It is widely known that the uniform distribution of photocatalyst without aggregation increases the surface area, thereby leading to the large number of active sites for photocatalysis. In addition, it is favorable for high permeate flux. Thus, the uniform distribution of TiO_2 on membrane without severe aggregation might contribute to the enhanced performance of photocatalytic membrane. The cross-sectional SEM images in Figure 4a,b show the macroporous structure of the bare Al_2O_3 membrane. Figure 4c,d reveals that the cross-section of the TiO_2 -deposited Al_2O_3 membrane is not significantly different from that of the bare membrane as a result of the deposition of a very thin TiO_2 film, as seen in the magnified image in Figure 4d.

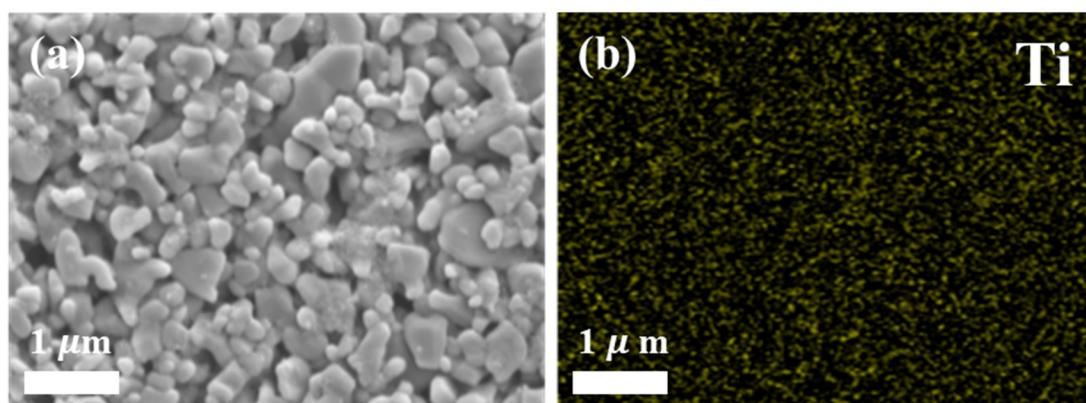


Figure 3. (a) Surface SEM image and (b) the corresponding EDS elemental (Ti) mapping image of POEM-directed TiO_2 films on Al_2O_3 membrane.

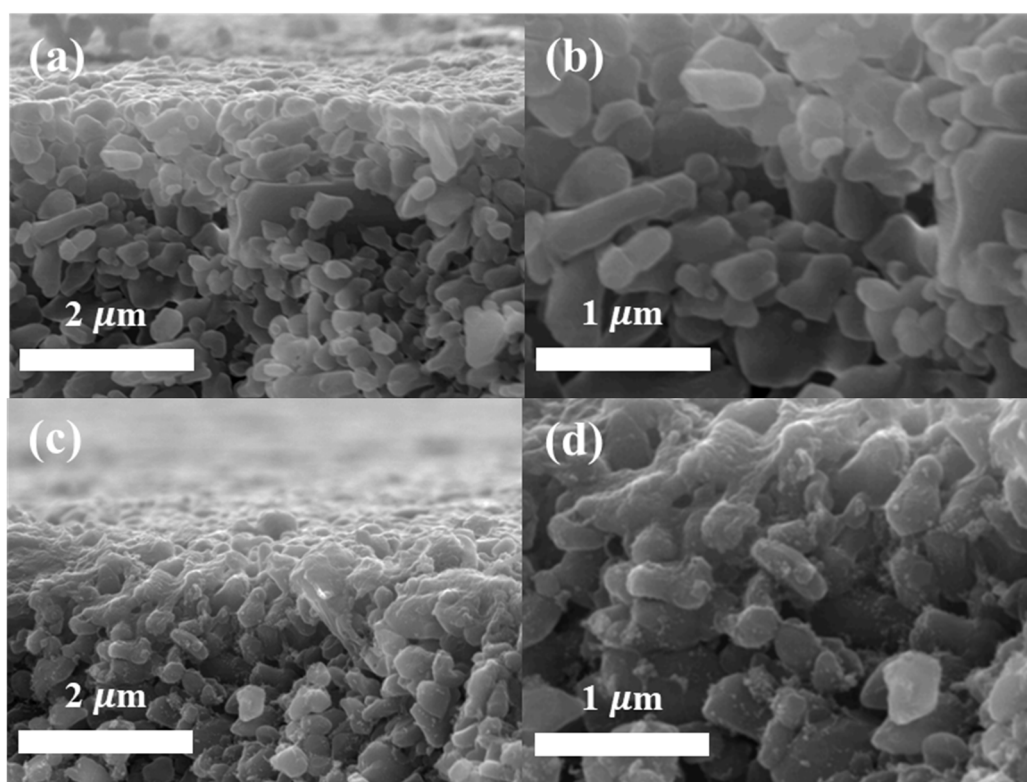


Figure 4. Cross sectional SEM images of the (a,b) bare Al_2O_3 membrane and (c,d) POEM-directed TiO_2 film on the Al_2O_3 membrane.

TEM and HR-TEM analyses were performed to characterize the crystalline properties and morphology of the TiO_2 film. The TEM image in Figure 5a confirmed that the POEM-templated TiO_2 structure is composed of uniform and well-interconnected nanoparticles. The HR-TEM and selected area electron diffraction (SAED) pattern in Figure 5b reveal that the TiO_2 structure is highly crystalline with a d -spacing value of approximately 0.35 nm, consistent with the (101) plane of the anatase TiO_2 phase. In general, these results indicate that the POEM-assisted TiO_2 structure is highly crystalline and well organized.

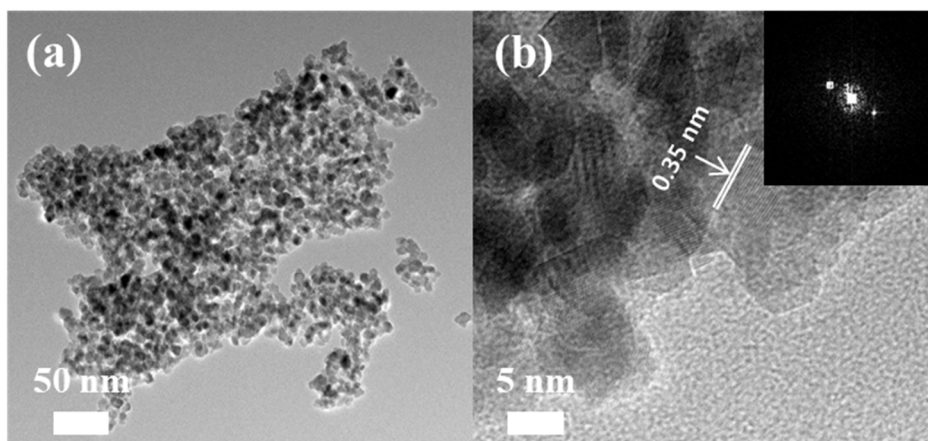


Figure 5. (a) Transmission electron microscopy (TEM) image and (b) high resolution transmission electron microscopy (HR-TEM) image (inset: selected area electron diffraction (SAED) pattern) of the TiO_2 film templated by POEM.

For detailed characterization of the crystalline properties, XRD analysis was conducted for the POEM-directed TiO_2 film deposited on the Al_2O_3 membrane, as shown in Figure 6. The sharp diffraction peaks are attributed to the TiO_2 and Al_2O_3 phases. The highly crystalline Al_2O_3 patterns marked in Figure 6 match the α -phase of alumina (Al_2O_3) (JCPDS Card No. 10-0173). The TiO_2 peaks at $2\theta = 25.5, 37.7$ and 61.2° correspond to the (101), (004), and (115) planes of anatase TiO_2 (JCPDS Card No. 21-1272). The anatase phase is widely known to be more effective for photocatalytic reactions than the rutile and brookite phases [9,19]. From the XRD results, it was concluded that the organic species were completely removed and that a highly crystalline anatase TiO_2 structure was obtained after calcination at 450°C .

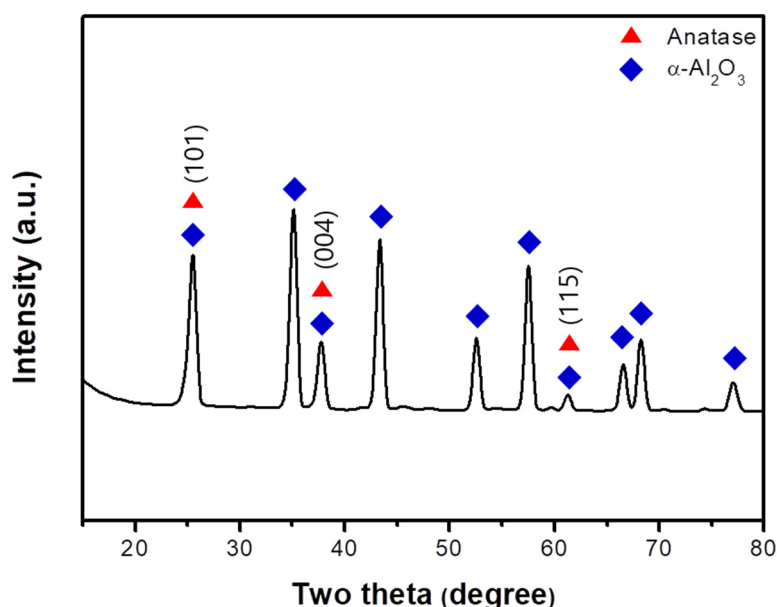


Figure 6. X-ray diffraction (XRD) pattern of the POEM-directed TiO_2 film on the Al_2O_3 membrane.

The three-dimensional morphology and structure of the POEM-directed TiO_2 film on the Al_2O_3 membrane and the bare Al_2O_3 membrane were investigated by AFM analysis. The topographical images and root-mean-square roughness (R_{rms}) of the membranes were obtained, as shown in Figure 7. The R_{rms} value for the bare Al_2O_3 membrane was 24.83 nm, resulting from its macroporous morphology.

With the introduction of a TiO_2 film templated by POEM, the value for the $\text{TiO}_2/\text{Al}_2\text{O}_3$ membrane was reduced to 5.56 nm. The decreased surface roughness is thus the result of the formation of a uniform TiO_2 structure on the macroporous Al_2O_3 membrane.

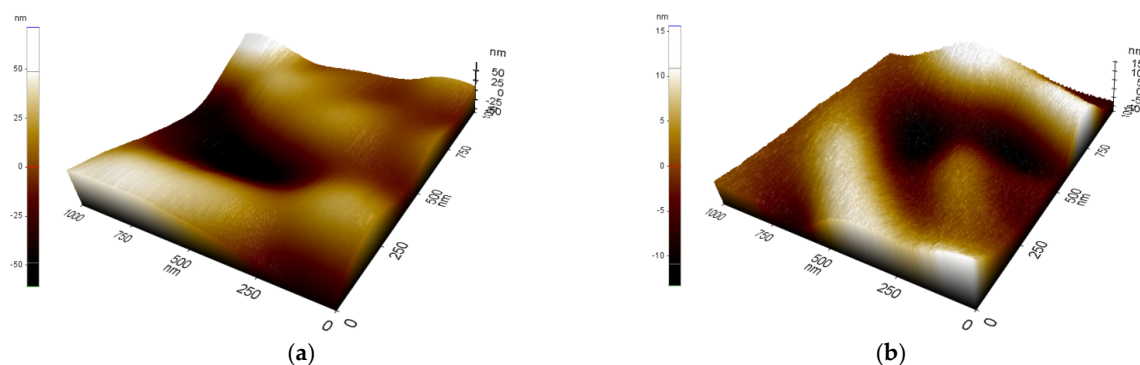


Figure 7. Atomic force microscopy (AFM) images of the (a) bare Al_2O_3 membrane and (b) Poly(oxyethylene methacrylate) (POEM)-directed TiO_2 film on the Al_2O_3 membrane.

3.2. Pure Water Permeability and Antifouling Properties

Table 1 shows the permeability of the bare Al_2O_3 and $\text{TiO}_2/\text{Al}_2\text{O}_3$ composite membranes for DI water after 2.5 h of filtration. A significant decline in the membrane permeability was observed after depositing a TiO_2 layer on the Al_2O_3 membrane support. In the absence of UV illumination, the permeability of the Al_2O_3 membrane was $65.2 \text{ L m}^{-2} \text{ h}^{-1} \text{ bar}^{-1}$, which was reduced to $9.9 \text{ L m}^{-2} \text{ h}^{-1} \text{ bar}^{-1}$ for the POEM-directed $\text{TiO}_2/\text{Al}_2\text{O}_3$ composite membrane. Such a reduction of the membrane permeability is attributed to the increased membrane resistance against the water flow upon significant reduction of the membrane pore size [20,21]. However, exposure to UV illumination enhanced the membrane permeability of both membranes. The permeability of the bare Al_2O_3 membrane and $\text{TiO}_2/\text{Al}_2\text{O}_3$ composite membrane under UV illumination increased to 71.5 and $14.2 \text{ L m}^{-2} \text{ h}^{-1} \text{ bar}^{-1}$, respectively. Such a membrane permeability enhancement can be resulted from improvement of the membrane wettability or higher water temperature induced by the UV irradiation [15,22]. The TiO_2 coating layer can improve surface hydrophilicity under UV radiation due to the production of the hydroxyl groups on membrane [23]. In addition, temperature increase can reduce water viscosity, thereby increasing membrane permeability [22]. To distinguish this effect, membrane permeability measured experimentally was compared with the calculated one by Darcy's equation (Equation (1)) at elevated temperature under UV irradiation at the end of filtration. For the bare membrane under UV irradiation, there is no difference in permeability between measured and calculated value (71.4 vs. $71.5 \text{ L m}^{-2} \text{ h}^{-1} \text{ bar}^{-1}$). This indicates that temperature played a dominant role in determining membrane permeability. For the $\text{TiO}_2/\text{Al}_2\text{O}_3$ composite membrane, membrane permeability measured was $14.2 \text{ L m}^{-2} \text{ h}^{-1} \text{ bar}^{-1}$, but the one calculated at the temperature increased by UV irradiation was $10.5 \text{ L m}^{-2} \text{ h}^{-1} \text{ bar}^{-1}$. Considering membrane permeability measured with the composite membrane ($9.9 \text{ L m}^{-2} \text{ h}^{-1} \text{ bar}^{-1}$), contribution of temperature increase to membrane permeability was relatively low compared to the bare membrane. Measurements of water temperature in the permeation line revealed a $5 \pm 1^\circ \text{C}$ increase with bare Al_2O_3 membrane (about 31°C). Increased water temperatures reduce the viscosity, thereby increasing the membrane permeability [22]. For the $\text{TiO}_2/\text{Al}_2\text{O}_3$ composite membrane, the water temperature increase was relatively small as about 3°C under UV illumination (about 29°C). A possible explanation is that the TiO_2 film on the Al_2O_3 membrane can support absorbing the UV light and reduce heat dissipation [15,22].

Table 1. Comparison of pure water permeability for bare Al₂O₃ membrane and Poly(oxyethylene methacrylate) (POEM)-directed TiO₂/Al₂O₃ composite membrane during filtration (with and without ultraviolet (UV) illumination).

□	Permeability (L m ⁻² h ⁻¹ bar ⁻¹)	
	Bare Al ₂ O ₃ Membrane	TiO ₂ /Al ₂ O ₃ Composite Membrane
Without UV	65.2	9.9
With UV	71.5	14.2

Figure 8 compares the effect of the permeate flux on the membrane fouling for both the bare Al₂O₃ and TiO₂/Al₂O₃ composite membranes in the absence and presence of UV illumination after filtration for 1 day. In the absence of UV illumination, the extent of the flux decline was lower for the TiO₂/Al₂O₃ composite membrane than for the bare Al₂O₃ membrane. The flux decline was ~89.6% lower on the TiO₂/Al₂O₃ composite membrane than on the bare Al₂O₃ membrane (1.25 vs. 0.13 LMH h⁻¹). The higher fouling rate in the bare Al₂O₃ membrane results from the higher probability of pore fouling in the larger pores of the bare membrane than in the smaller pores of the TiO₂/Al₂O₃ composite membrane [23]. The previous results also confirmed that the membrane permeability decreased significantly after immobilizing a TiO₂ layer on the Al₂O₃ membrane support, as shown in Table 1. The benefits of applying the POEM template become obvious upon exposing the membranes to UV illumination. In fact, no flux decline was observed for the POEM-directed TiO₂/Al₂O₃ composite membrane under UV illumination. In contrast, severe membrane fouling was observed in the bare Al₂O₃ membrane under UV illumination, with a ~51.2% decay in the permeate flux relative to that in the absence of UV illumination (2.57 vs. 1.25 LMH h⁻¹). The higher fouling rate on the bare Al₂O₃ membrane under UV illumination is attributed to the formation of a cake layer on the membrane surface [15]. Although photolysis phenomena are likely involved during organic degradation on the bare Al₂O₃ membrane [24,25], photolysis itself may not be sufficient to remove the cake layer on the membrane.

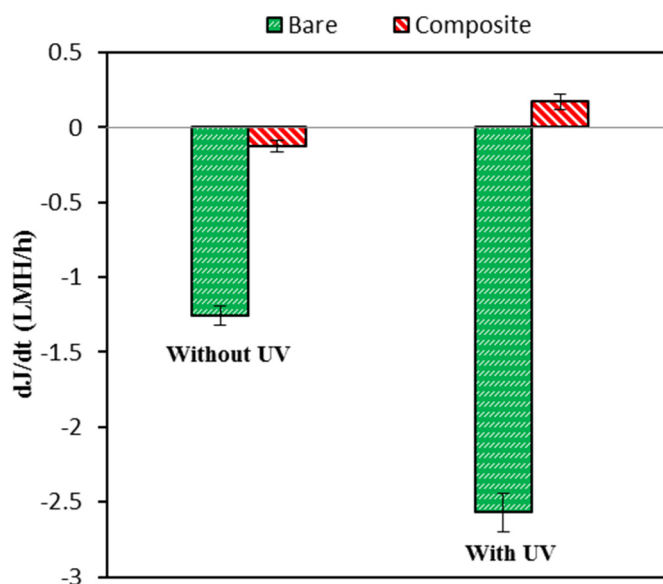


Figure 8. Comparison of the membrane fouling rate for the bare Al₂O₃ membrane and Poly(oxyethylene methacrylate) (POEM)-directed TiO₂/Al₂O₃ composite membrane during filtration in the presence (With UV) and absence (Without UV) of ultraviolet (UV) illumination (filtration time: 24 h).

3.3. Organic Dye Removal Efficiency

Figure 9 shows the dye adsorption curves for both the bare Al_2O_3 membrane and $\text{TiO}_2/\text{Al}_2\text{O}_3$ composite membrane. In the absence of UV illumination, the $\text{TiO}_2/\text{Al}_2\text{O}_3$ composite membrane shows a higher adsorption capacity than the bare Al_2O_3 membrane, which was almost saturated after 9 h of filtration. The $\text{TiO}_2/\text{Al}_2\text{O}_3$ composite membrane presents a higher dye organic removal efficiency (~20%) than the bare Al_2O_3 membrane after the same filtration time. The higher adsorption capacity of the $\text{TiO}_2/\text{Al}_2\text{O}_3$ composite membrane arises mainly from complementary cavities and rebinding sites on the membrane assisted by the POEM template [26]. The advantages of the presence of such a well-organized TiO_2 film were further observed upon carrying out the membrane filtration under UV illumination (Figure 9b). About 96% of dye removal efficiency was observed with the $\text{TiO}_2/\text{Al}_2\text{O}_3$ composite membrane after 24 h of filtration. The catalytic active sites offered by the POEM template favor the membrane photocatalytic activity. In contrast, only ~40% of the organic dye was removed by the bare Al_2O_3 membrane under UV illumination [15]. However, ~89% of organic removal efficiency was achieved after 6.5 h membrane filtration, probably due to photolysis phenomena occurring on the membrane surface [25]. Moreover, the formed cake layer may act as a secondary membrane, thus improving the organic dye removal by membrane filtration [15].

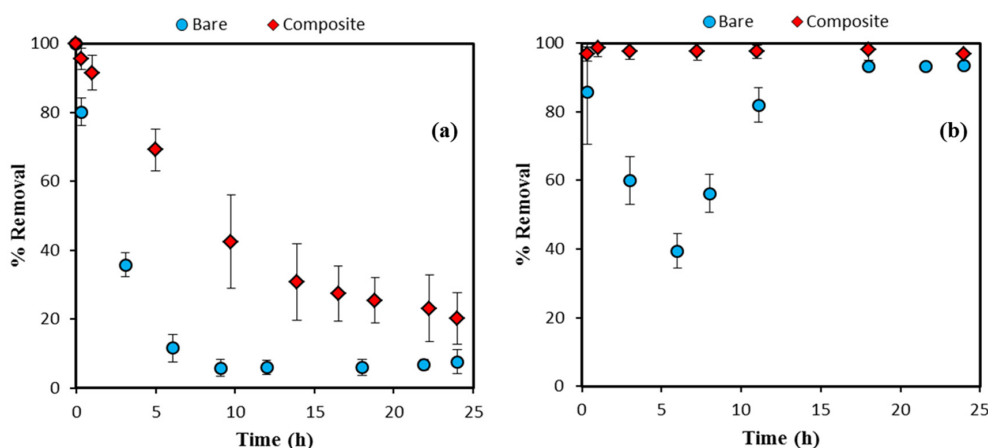


Figure 9. Organic dye removal efficiency of bare Al_2O_3 membrane and POEM-directed $\text{TiO}_2/\text{Al}_2\text{O}_3$ composite membrane in the (a) absence and (b) presence of UV illumination.

4. Conclusions

A nanostructured photocatalytic $\text{TiO}_2/\text{Al}_2\text{O}_3$ composite membrane was successfully fabricated using a POEM polymer template through a sol–gel process. The hydrophilic POEM chains interact strongly with the TiO_2 precursor (TTIP) to form uniform POEM/TTIP hybrids. Upon calcination at 450 °C, TTIP is transformed into highly crystalline anatase TiO_2 while the organic POEM is completely decomposed. The well-organized structure and morphology of the TiO_2 film were confirmed by HR-TEM, SEM, XRD, and AFM analyses. A homogenous distribution of the catalytic sites on the membrane surface was achieved, exhibiting a higher adsorption capacity toward Congo red (a model organic dye) than that of the bare Al_2O_3 membrane. Under UV illumination, the $\text{TiO}_2/\text{Al}_2\text{O}_3$ composite membrane showed 96% organic removal efficiency along with effective fouling mitigation.

Acknowledgments: This work was supported by an Inha University research grant.

Author Contributions: Jeonghwan Kim and Jong Hak Kim conceived and designed the experiments; Rizwan Ahmad and Jin Kyu Kim performed the experiments; Rizwan Ahmad, Jin Kyu Kim, Jong Hak Kim and Jeonghwan Kim analyzed the data; Jeonghwan Kim, Jong Hak Kim, Rizwan Ahmad and Jin Kyu Kim wrote the paper.

Conflicts of Interest: The authors declare no conflict of interest.

References

1. Liu, G.; Han, K.; Ye, H.; Zhu, C.; Gao, Y.; Liu, Y.; Zhou, Y. Graphene oxide/triethanolamine modified titanate nanowires as photocatalytic membrane for water treatment. *Chem. Eng. J.* **2017**, *320*, 74–80. [[CrossRef](#)]
2. Zhao, H.; Li, H.; Yu, H.; Chang, H.; Quan, X.; Chen, S. CNTs-TiO₂/Al₂O₃ composite membrane with a photocatalytic function: Fabrication and energetic performance in water treatment. *Sep. Purif. Technol.* **2013**, *116*, 360–365. [[CrossRef](#)]
3. Aslam, M.; McCarty, P.L.; Shin, C.; Bae, J.; Kim, J. Low energy single-staged anaerobic fluidized bed ceramic membrane bioreactor (AFCMR) for wastewater treatment. *Bioresour. Technol.* **2017**, *240*, 33–41. [[CrossRef](#)] [[PubMed](#)]
4. Ko, C.-C.; Chen, C.-H.; Chen, Y.-R.; Wu, Y.-H.; Lu, S.-C.; Hu, F.-C.; Li, C.-L.; Tung, K.-L. Increasing the performance of vacuum membrane distillation using micro-structured hydrophobic aluminum hollow fiber membranes. *Appl. Sci.* **2017**, *7*, 357. [[CrossRef](#)]
5. Hofs, B.; Ogier, J.; Vries, D.; Beerendonk, E.F.; Cornelissen, E.R. Comparison of ceramic and polymeric membrane permeability and fouling using surface water. *Sep. Purif. Technol.* **2011**, *79*, 365–374. [[CrossRef](#)]
6. Ahmad, R.; Kim, J.K.; Kim, J.H.; Kim, J. Effect of polymer template on structure and membrane fouling of TiO₂/Al₂O₃ composite membranes for wastewater treatment. *J. Ind. Eng. Chem.* **2017**, *57*, 55–63. [[CrossRef](#)]
7. Ma, N.; Zhang, Y.; Quan, X.; Fan, X.; Zhao, H. Performing a microfiltration integrated with photocatalysis using an Ag-TiO₂/HAP/Al₂O₃ composite membrane for water treatment: Evaluating effectiveness for humic acid removal and anti-fouling properties. *Water Res.* **2010**, *44*, 6104–6114. [[CrossRef](#)] [[PubMed](#)]
8. Goei, R.; Lim, T.-T. Asymmetric TiO₂ hybrid photocatalytic ceramic membrane with porosity gradient: Effect of structure directing agent on the resulting membranes architecture and performances. *Ceram. Int.* **2014**, *40*, 6747–6757. [[CrossRef](#)]
9. Ahmad, R.; Ahmad, Z.; Khan, A.U.; Mastoi, N.R.; Aslam, M.; Kim, J. Photocatalytic systems as an advanced environmental remediation: Recent developments, limitations and new avenues for applications. *J. Environ. Chem. Eng.* **2016**, *4*, 4143–4164. [[CrossRef](#)]
10. Kwon, S.; Fan, M.; Cooper, A.T.; Yang, H. Photocatalytic applications of micro- and nano-TiO₂ in environmental engineering. *Crit. Rev. Env. Sci. Technol.* **2008**, *38*, 197–226. [[CrossRef](#)]
11. Gao, Y.; Hu, M.; Mi, B. Membrane surface modification with TiO₂-graphene oxide for enhanced photocatalytic performance. *J. Membr. Sci.* **2014**, *455*, 349–356. [[CrossRef](#)]
12. Romanos, G.E.; Athanasekou, C.P.; Katsaros, F.K.; Kanellopoulos, N.K.; Dionysiou, D.D.; Likodimos, V.; Falaras, P. Double-side active TiO₂-modified nanofiltration membranes in continuous flow photocatalytic reactors for effective water purification. *J. Hazard. Mater.* **2012**, *211–212*, 304–316. [[CrossRef](#)] [[PubMed](#)]
13. Athanasekou, C.P.; Romanos, G.E.; Katsaros, F.K.; Kordatos, K.; Likodimos, V.; Falaras, P. Very efficient composite titania membranes in hybrid ultrafiltration/photocatalysis water treatment processes. *J. Membr. Sci.* **2012**, *392*, 192–203. [[CrossRef](#)]
14. Athanasekou, C.P.; Morales-Torres, S.; Likodimos, V.; Romanos, G.E.; Pastrana-Martinez, L.M.; Falaras, P.; Dionysiou, D.D.; Faria, J.L.; Figueiredo, J.L.; Silva, A.M.T. Prototype composite membranes of partially reduced graphene oxide/TiO₂ for photocatalytic ultrafiltration water treatment under visible light. *Appl. Catal. B Environ.* **2014**, *158*, 361–372. [[CrossRef](#)]
15. Ahmad, R.; Kim, J.K.; Kim, J.H.; Kim, J. Well-organized, mesoporous nanocrystalline TiO₂ on alumina membranes with hierarchical architecture: Antifouling and photocatalytic activities. *Catal. Today* **2017**, *282*, 2–12. [[CrossRef](#)]
16. Goei, R.; Dong, Z.; Lim, T.-T. High-permeability pluronic-based TiO₂ hybrid photocatalytic membrane with hierarchical porosity: Fabrication, characterizations and performances. *Chem. Eng. J.* **2013**, *228*, 1030–1039. [[CrossRef](#)]
17. Choi, H.; Stathatos, E.; Dionysiou, D.D. Sol-gel preparation of mesoporous photocatalytic TiO₂ films and TiO₂/Al₂O₃ composite membranes for environmental applications. *Appl. Catal. B Environ.* **2006**, *63*, 60–67. [[CrossRef](#)]
18. Zheng, M.-P.; Gu, M.-Y.; Jin, Y.-P.; Wang, H.-H.; Zu, P.-F.; Tao, P.; He, J.-B. Effects of PVP on structure of TiO₂ prepared by the sol-gel process. *Mater. Sci. Eng. B* **2001**, *87*, 197–201. [[CrossRef](#)]

19. Li, G.; Richter, C.P.; Milot, R.L.; Cai, L.; Schmittenmaer, C.A.; Crabtree, R.H.; Brudvig, G.W.; Batista, V.S. Synergistic effect between anatase and rutile TiO₂ nanoparticles in dye-sensitized solar cells. *Dalton Trans.* **2009**, *45*, 10078–10085. [[CrossRef](#)] [[PubMed](#)]
20. Alem, A.; Sarpoolaky, H.; Keshmiri, M. Titania ultrafiltration membrane: Preparation, characterization and photocatalytic activity. *J. Eur. Ceram. Soc.* **2009**, *29*, 629–635. [[CrossRef](#)]
21. Choi, H.; Stathatos, E.; Dionysiou, D.D. Photocatalytic TiO₂ films and membranes for the development of efficient wastewater treatment and reuse systems. *Desalination* **2007**, *202*, 199–206. [[CrossRef](#)]
22. Guo, B.; Pasco, E.V.; Xagorarakis, I.; Tarabara, V.V. Virus removal and inactivation in a hybrid microfiltration–UV process with a photocatalytic membrane. *Sep. Purif. Technol.* **2015**, *149*, 245–254. [[CrossRef](#)]
23. Mendret, J.; Hatat-Fraile, M.; Rivallin, M.; Brosillon, S. Hydrophilic composite membranes for simultaneous separation and photocatalytic degradation of organic pollutants. *Sep. Purif. Technol.* **2013**, *111*, 9–19. [[CrossRef](#)]
24. Ahmad, R.; Kim, J.K.; Kim, J.H.; Kim, J. In-situ TiO₂ formation and performance on ceramic membranes in photocatalytic membrane reactor. *Membr. J.* **2017**, *27*, 328–335. [[CrossRef](#)]
25. Kamel, D.; Sihem, A.; Halima, C.; Tahar, S. Decolourization process of an azoïque dye (congo red) by photochemical methods in homogeneous medium. *Desalination* **2009**, *247*, 412–422. [[CrossRef](#)]
26. Zhao, K.; Feng, L.; Lin, H.; Fu, Y.; Lin, B.; Cui, W.; Li, S.; Wei, J. Adsorption and photocatalytic degradation of methyl orange imprinted composite membranes using TiO₂/calcium alginate hydrogel as matrix. *Catal. Today* **2014**, *236*, 127–134. [[CrossRef](#)]



© 2017 by the authors. Licensee MDPI, Basel, Switzerland. This article is an open access article distributed under the terms and conditions of the Creative Commons Attribution (CC BY) license (<http://creativecommons.org/licenses/by/4.0/>).